Modeling spatial and temporal variabilities in hyperspectral image unmixing

Pierre-Antoine THOUVENIN
PhD defense, IRIT/INP-ENSEEIHT, Toulouse

Supervisor	Nicolas DOBIGEON	Professor at IRIT/INP-ENSEEIHT, Toulouse
Co-supervisor	Jean-Yves TOURNERET	Professor at IRIT/INP-ENSEEIHT, Toulouse
DGA contact	Véronique SERFATY	

University of Toulouse, IRIT/INP-ENSEEIHT

October 17, 2017

A brief introduction to hyperspectral unmixing

- Airborne/spaceborne hyperspectral (HS) images: high spectral resolution (10 nm), comparatively lower spatial resolution (20 m $\times$ 20 m);

A brief introduction to hyperspectral unmixing

- Airborne/spaceborne hyperspectral (HS) images: high spectral resolution (10 nm), comparatively lower spatial resolution (20 m × 20 m);

Hyperspectral cube

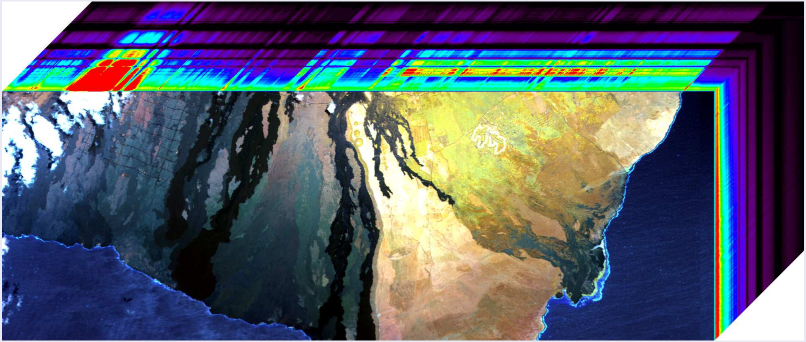

A brief introduction to hyperspectral unmixing

- Airborne/spaceborne hyperspectral (HS) images: high spectral resolution (10 nm), comparatively lower spatial resolution (20 m $\times$ 20 m);
- Observations: mixture of several spectra corresponding to distinct materials (*endmembers*);

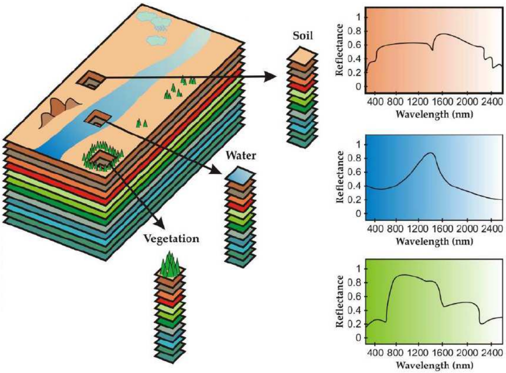

Figure 1: Hyperspectral unmixing: an illustration (taken from [Bio+12]).

A brief introduction to hyperspectral unmixing

- Airborne/spaceborne hyperspectral (HS) images: high spectral resolution (10 nm), comparatively lower spatial resolution (20 m × 20 m);
- Observations: mixture of several spectra corresponding to distinct materials (*endmembers*);
- Endmembers present in unknown proportions in each pixel (*abundance*, quantitative spatial mapping).

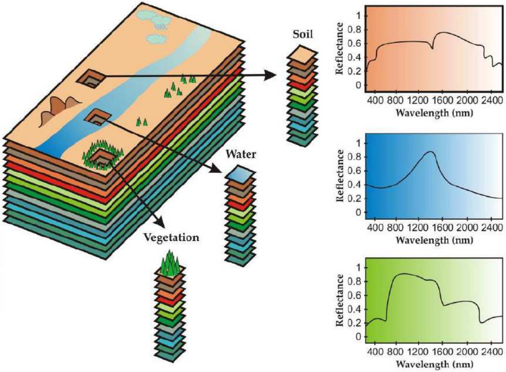

Figure 1: Hyperspectral unmixing: an illustration (taken from [Bio+12]).

Linear mixture model

Linear mixture model

Traditionally, observations are represented by a linear combination of the unknown endmembers [Bio+12]

$$\forall n \in \{1, \dots N\}, \quad \mathbf{y}_n = \sum_{r=1}^{R} a_{rn}\mathbf{m}_r + \mathbf{b}_n \tag{1}$$

$$\mathbf{Y} = \mathbf{M}\mathbf{A} + \mathbf{B} \tag{2}$$

Constraints (physical interpretability)

$$\mathbf{A} \succeq \mathbf{0}_{R,N}, \quad \mathbf{A}^{\mathsf{T}}\mathbf{1}_R = \mathbf{1}_N, \quad \mathbf{M} \succeq \mathbf{0}_{L,R} \tag{3}$$

- Several models are available in the literature to capture more complex interations between light and matter [Hal+11; Dob+14; HPG14; ADT14] (e.g. multiple reflections).
- A given material is assumed to be fully characterized by a single signature.

Endmember variability

- Endmembers possibly affected by local environmental factors, varying acquisition conditions: spectral variability;
- Spatial variability: significant source of errors when estimating the abundance coefficients;
- Error propagation within unsupervised unmixing procedures
  ⇝ need for appropriate models.

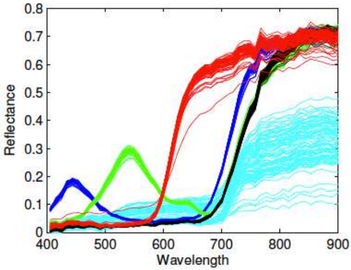

(a) Endmember variability (taken from [Gad+13])

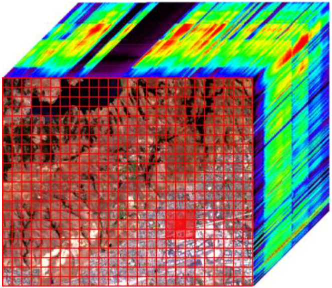

(b) Spatial variability

Figure 2: Endmember spatial variability: an illustration.

Temporal endmember variability

- Variability: a prominent issue when considering multi-temporal hyperspectral (MTHS) images
  - ▷ varying acquisition conditions;
  - ▷ natural evolution of the scene (e.g. water, vegetation).

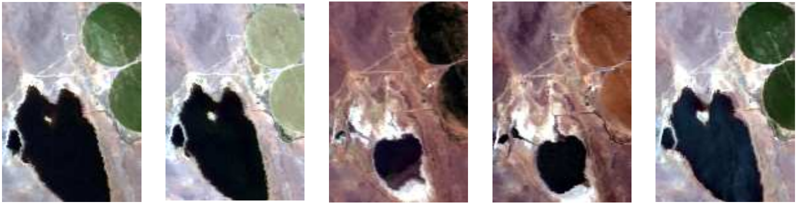

(a) 10/04/14 (b) 02/06/14 (c) 19/09/14 (d) 17/11/14 (e) 29/04/15

Figure 3: An example of a sequence of hyperspectral images, acquired at different time instants.

Variability accounting methods

Essentially two modeling paradigms

Variability accounting methods

Essentially two modeling paradigms

- Automated endmember bundles (AEB) [Som+12; Rob+98; Goe+13]
  - ▷ unmixing relies on spectral libraries, either extracted from the data or *a priori* available.

Variability accounting methods

Essentially two modeling paradigms

- Automated endmember bundles (AEB) [Som+12; Rob+98; Goe+13]
  - ▷ unmixing relies on spectral libraries, either extracted from the data or *a priori* available.
- Normal compositional model (NCM) [Ech+10; HDT15], Beta compositional model (BCM) [Du+14]
  - ▷ endmembers modeled as realizations of random vectors.

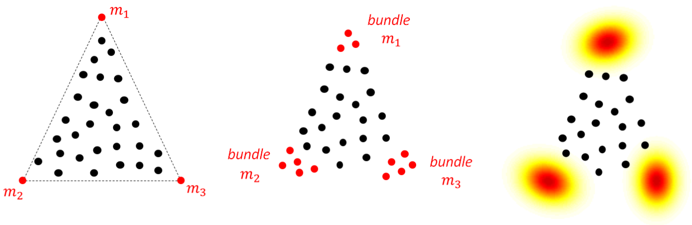

Figure 4: Different representations of endmember variability within the simplex enclosing the data (illustration taken from [HDT15]).

Overview

1. A perturbed LMM to account for spatial variability
2. Online unmixing of MTHS images
3. A partially asynchronous distributed unmixing algorithm
4. Conclusion and perspectives

Overview

1. A perturbed LMM to account for spatial variability
   - Model and problem formulation
   - Experiments on real data

2. Online unmixing of MTHS images

3. A partially asynchronous distributed unmixing algorithm

4. Conclusion and perspectives

Model

Perturbed LMM (PLMM) [Thouvenin *et al.*, IEEE TSP 2016]

Observations are represented as a linear combination of possibly perturbed endmembers

$$\forall n \in \{1, \ldots, N\}, \quad \mathbf{y}_n = \sum_{r=1}^{R} a_{r,n} \left(\mathbf{m}_r + \mathbf{dm}_{r,n}\right) + \mathbf{b}_n \tag{4}$$

$$\mathbf{Y} = \mathbf{MA} + \underbrace{\left[\ \mathbf{dM}_1 \mathbf{a}_1 \ \middle|\ \ldots\ \middle|\ \mathbf{dM}_N \mathbf{a}_N\ \right]}_{\boldsymbol{\Delta}} + \mathbf{B} \tag{5}$$

▷ In practice, problem tractable for a limited number of pixels per image.

Constraints

$$\begin{gathered} \mathbf{A} \succeq \mathbf{0}_{R,N}, \quad \mathbf{A}^{\mathsf{T}} \mathbf{1}_R = \mathbf{1}_N, \quad \mathbf{M} \succeq \mathbf{0}_{L,R} \\ \mathbf{M} + \mathbf{dM}_n \succeq \mathbf{0}_{L,R}, \quad \|\mathbf{dM}_n\|_{\mathrm{F}} \leq \nu, \quad \forall n \in \{1, \ldots, N\} \end{gathered} \tag{6}$$

▷ This model can be used to formulate a constrained optimization problem.

Problem formulation

Optimization problem

$$(\mathbf{M}^*, \mathbf{dM}^*, \mathbf{A}^*) \in \underset{\mathbf{M}, \mathbf{dM}, \mathbf{A}}{\arg\min} \left\{ F(\mathbf{M}, \mathbf{dM}, \mathbf{A}) \text{ s.t. } (6) \right\} \tag{7}$$

$$F(\mathbf{M}, \mathbf{dM}, \mathbf{A}) = \underbrace{\frac{1}{2} \|\mathbf{Y} - \mathbf{MA} - \mathbf{\Delta}\|_{\mathrm{F}}^2}_{\text{data fitting term}} + \underbrace{\alpha\Phi(\mathbf{A}) + \beta\Psi(\mathbf{M}) + \gamma\Upsilon(\mathbf{dM})}_{\text{penalizations}}$$

Choice of the penalization terms:

- Φ: promotes spatially smooth abundances;
- Ψ: restrains the volume occupied by the $R-1$ simplex enclosing the data;
- Υ: limits the energy of the captured variability.

Alternating minimization adopted: ADMM steps within a block coordinate descent (BCD), PALM (Proximal alternating linearized minimization [BST13]).

Penalization terms

Abundance penalization

Promote spatially smooth variations [CRH14]

$$\Phi(\mathbf{A}) = \frac{1}{2} \|\mathbf{AH}\|_{\mathrm{F}}^2 \tag{8}$$

where $\mathbf{H} \in \mathbb{R}^{N \times 4N}$ computes the difference between the abundances of a pixel and those of its neighbors.

Endmember penalization

Approximate the volume occupied by the $(R-1)$-simplex enclosing the data [Ber+04]:

$$\Psi(\mathbf{M}) = \frac{1}{2} \sum_{i \neq j} \|\mathbf{m}_i - \mathbf{m}_j\|_2^2. \tag{9}$$

Estimation algorithm (I)

Two estimation algorithms considered: BCD/ADMM and PALM algorithms.

- BCD/ADMM unmixing algorithm [Thouvenin *et al.*, IEEE TSP 2016]
  - ▷ no convergence proof (approximate BCD).

Algorithm 1: PLMM-unmixing: a BCD/ADMM algorithm. Each sub-problem resulting from the decomposition of the optimization steps is solved by ADMM.

Data: $\mathbf{Y}$, $\mathbf{A}^0$, $\mathbf{M}^0$, $\mathbf{dM}^0$

begin

$k \leftarrow 0$;

while *stopping criterion not satisfied* **do**

(a) $$\mathbf{A}^{k+1} = \arg\min_{\mathbf{A}} F\left(\mathbf{M}^k, \mathbf{dM}^k, \mathbf{A}\right) ;$$

(b) $$\mathbf{M}^{k+1} = \arg\min_{\mathbf{M}} F\left(\mathbf{M}, \mathbf{dM}^k, \mathbf{A}^{k+1}\right) ;$$

(c) $$\mathbf{dM}^{k+1} = \arg\min_{\mathbf{dM}} F\left(\mathbf{M}^{k+1}, \mathbf{dM}, \mathbf{A}^{k+1}\right) ;$$

$k \leftarrow k + 1$;

Result: $\mathbf{A}^{k+1}$, $\mathbf{M}^{k+1}$, $\mathbf{dM}^{k+1}$

Estimation algorithm (II)

- PALM algorithm [BST13; CPR16]
  - ▷ sequence of iterates proved to converge to a critical point of the objective function (based on the Kurdyka-Łojasiewicz property).

Algorithm 2: PALM algorithm to estimate the parameters of the PLMM.

Data: $\mathbf{Y}$, $\mathbf{A}^0$, $\mathbf{M}^0$, $\mathbf{dM}^0$

begin

$k \leftarrow 0$;

while *stopping criterion not satisfied* **do**

`// Abundance update`

for $n = 1$ **to** N **do**

(a) $$\mathbf{a}_n^{k+1} = \text{prox}_{\iota_{\mathcal{S}_R}}\left(\mathbf{a}_n^k - \frac{1}{\eta_n^k}\nabla_{\mathbf{a}_n} f\left(\mathbf{a}_n^k, \mathbf{M}^k, \mathbf{dM}_n^k\right)\right);$$

`// Endmember update`

(b) $$\mathbf{M}^{k+1} = \text{prox}_{\iota_{\{\cdot \succeq \mathbf{C}^k\}}}\left(\mathbf{M}^k - \frac{1}{\mu^k}\nabla_{\mathbf{M}} F\left(\mathbf{A}^{k+1}, \mathbf{M}^k, \mathbf{dM}^k\right)\right), \ \mathbf{C}^k = \max\{\mathbf{0}, \max_n -\mathbf{dM}_n^k\};$$

`// Variability update`

for $n = 1$ **to** N **do**

(c) $$\mathbf{dM}_n^{k+1} = \text{prox}_{\iota_{\{\|\cdot\|_F \leq \nu\}} + \iota_{\{\cdot \succeq -\mathbf{M}^{k+1}\}}}\left(\mathbf{dM}_n^k - \frac{1}{\nu_n^k}\nabla_{\mathbf{dM}_n} f\left(\mathbf{a}_n^{k+1}, \mathbf{M}^{k+1}, \mathbf{dM}_n^k\right)\right);$$

$k \leftarrow k + 1$;

Result: $\mathbf{A}^k$, $\mathbf{M}^k$, $\mathbf{dM}^k$

Experiments on real data (I)

Moffett scene:

- 50×50 image acquired over Moffett Field (CA) in 1997;
- scene partly composed of a lake and a coastal area;
- 189 out of the 224 available spectral bands are exploited (water absorption bands removal)
- previous studies available for this scene [Dob+09; Hal+11; EDT11]

Experiments on real data (II)

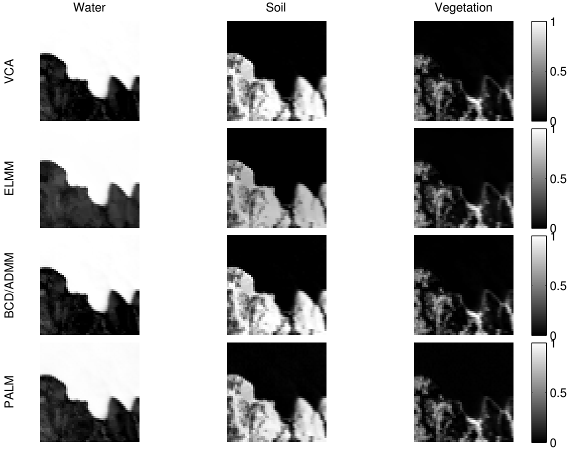

Figure 5: Abundance maps estimated for the Moffett scene.

Experiments on real data (III)

- Variability energy concentrated on interface areas (possible nonlinearities).

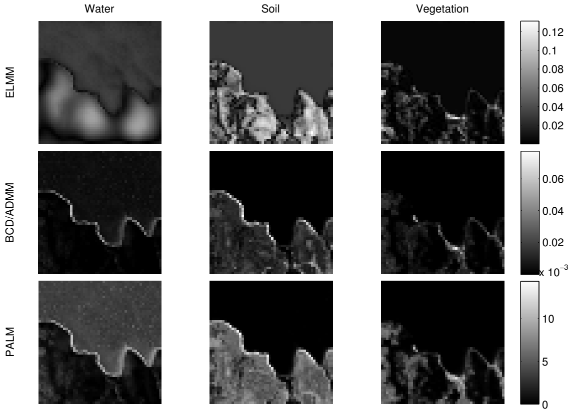

Figure 6: Spatial distribution of the variability w.r.t. each endmember estimated for the Moffett dataset. The maps are presented in terms of the variability energy for visualization purpose ($\|\mathbf{dm}_{r,n}\|_2/\sqrt{L}$ for the rth endmember in the nth pixel).

Experiments on real data (IV)

- Variability peaks: result from spectral bands with a poor SNR.
- Notable estimation improvement for the water signature.

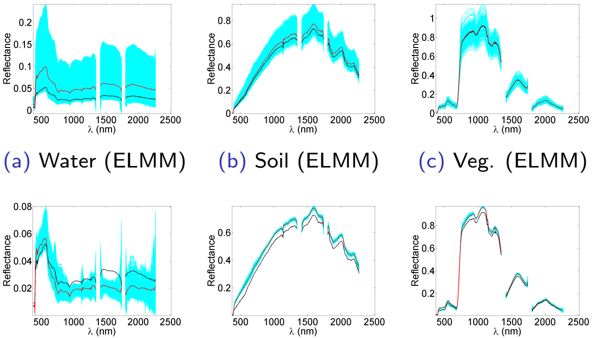

(a) Water (ELMM) (b) Soil (ELMM) (c) Veg. (ELMM)

(d) Water (PALM) (e) Soil (PALM) (f) Veg. (PALM)

Figure 7: Endmembers estimated for the Moffett scene (red lines), VCA in black, and variability in cyan.

Overview

1. A perturbed LMM to account for spatial variability

2. Online unmixing of MTHS images
   - Context and motivations
   - Model and problem formulation
   - Experiments on real data

3. A partially asynchronous distributed unmixing algorithm

4. Conclusion and perspectives

Context and motivations

- **Data:** multi-temporal hyperspectral (MTHS) images
  - ▷ similar materials expected to be observed over time;
  - ▷ exploit temporal information redundancy (possibly smooth variations of the parameters);
  - ▷ significant size of the data may preclude the use of batch procedures.
- Varying acquisition conditions may affect the shape and the amplitude of the endmembers.

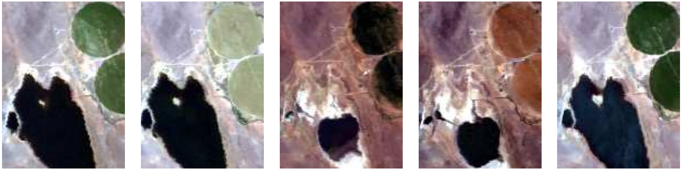

(a) 10/04/14 (b) 02/06/14 (c) 19/09/14 (d) 17/11/14 (e) 29/04/15

Figure 8: Sequence of hyperspectral images analyzed in this section.

Model

As a first approximation, endmember variability is assumed to be uniform on each image

$\rightsquigarrow$ significant reduction in the number of unknown parameters.

PLMM variant [Thouvenin *et al.*, IEEE TIP 2016]

$$\mathbf{Y}_t = (\mathbf{M} + \mathbf{dM}_t)\mathbf{A}_t + \mathbf{B}_t, \quad \forall t = 1, \dots, T \tag{10}$$

Constraints

$$\begin{gathered} \mathbf{M} \succeq \mathbf{0}_{L,R}, \quad \mathbf{A}_t \succeq \mathbf{0}_{R,N}, \quad \mathbf{A}_t^T \mathbf{1}_R = \mathbf{1}_N \\ \left\| \frac{1}{T} \sum_{t=1}^{T} \mathbf{dM}_t \right\|_F \leq \kappa, \quad \|\mathbf{dM}_t\|_F \leq \nu. \end{gathered} \tag{11}$$

Problem formulation

Proposed approach: online unmixing – the available data are sequentially processed to estimate the mixture parameters (based on [Mai+10])

$\rightsquigarrow$ problem formulated as a two stage stochastic program

Problem statement

$$\min_{\mathbf{M}\in[0,1]^{L\times R}} g(\mathbf{M}) = \mathbb{E}_{\mathbf{Y},\mathbf{A},\mathbf{dM}}\left[f\left(\mathbf{Y},\mathbf{M},\mathbf{A},\mathbf{dM}\right)\right] \text{ s.t. } (11)$$

$$f(\mathbf{Y},\mathbf{M},\mathbf{A},\mathbf{dM}) = \frac{1}{2}\|\mathbf{Y}-(\mathbf{M}+\mathbf{dM})\mathbf{A}\|_F^2 + \alpha\Phi(\mathbf{A}) + \beta\Psi(\mathbf{M}) + \gamma\Upsilon(\mathbf{dM}).$$

where Φ, and Υ promote smooth temporal variations of the associated parameters.

Stochastic approximation

$$g_t(\mathbf{M}) = \frac{1}{2t}\sum_{i=1}^{t}\|\mathbf{Y}_i-(\mathbf{M}+\mathbf{dM}_i)\mathbf{A}_i\|_F^2 + \beta\Psi(\mathbf{M})$$

$$= \frac{1}{t}\left[\frac{1}{2}\mathrm{Tr}(\mathbf{M}^T\mathbf{M}\mathbf{C}_t) + \mathrm{Tr}(\mathbf{M}^T\mathbf{D}_t)\right] + \beta\Psi(\mathbf{M}) + c.$$

Two stage stochastic program

Two stage stochastic program (see, e.g., [RX11])

- acquire an HS image $\mathbf{Y}_t$;
- estimate the corresponding abundance and variability terms, solution to a first optimization problem (first stage problem)

$$(\mathbf{A}_t, \mathbf{dM}_t) \in \underset{(\mathbf{A}, \mathbf{dM}) \in \mathcal{A}_R \times \mathcal{D}_t}{\arg\min} f(\mathbf{Y}_t, \mathbf{M}^{(t-1)}, \mathbf{A}, \mathbf{dM}); \tag{12}$$

- update the endmember matrix using the newly extracted information, as a solution to the second stage problem

$$\mathbf{M}^{(t)} = \underset{\mathbf{M} \in \mathcal{M}}{\arg\min}\, \hat{g}_t(\mathbf{M}). \tag{13}$$

Proposed algorithm
[Thouvenin *et al.*, IEEE TIP 2016]

Remark: a convergence result can be obtained (under milder assumptions than those considered in the manuscript) by interpreting the proposed algorithm as an instance of the BC-VMFB algorithm [CPR16].

Algorithm 3: Online unmixing algorithm.

Data: $\mathbf{M}^{(0)}$, $\mathbf{A}_0$, $\mathbf{dM}_0$, $\alpha > 0$, $\beta > 0$, $\gamma > 0$, $\xi \in]0,1]$

begin

$\mathbf{C}_0 \leftarrow \mathbf{0}_{R,R}$;

$\mathbf{D}_0 \leftarrow \mathbf{0}_{L,R}$;

$\mathbf{E}_0 \leftarrow \mathbf{0}_{L,R}$;

for $t = 1$ **to** T **do**

a — Random selection of an image $\mathbf{Y}_t$ (random permutation of the image sequence);

`// Abundance and variability estimation by PALM [BST13]`

b — $(\mathbf{A}_t, \mathbf{dM}_t) \in \underset{(\mathbf{A},\mathbf{dM}) \in \mathcal{A}_R \times \mathcal{D}_t}{\arg\min} f(\mathbf{Y}_t, \mathbf{M}^{(t-1)}, \mathbf{A}, \mathbf{dM})$;

$\mathbf{C}_t \leftarrow \xi \mathbf{C}_{t-1} + \mathbf{A}_t \mathbf{A}_t^T$;

$\mathbf{D}_t \leftarrow \xi \mathbf{D}_{t-1} + (\mathbf{dM}_t \mathbf{A}_t - \mathbf{Y}_t)\mathbf{A}_t^T$;

$\mathbf{E}_t \leftarrow \xi \mathbf{E}_{t-1} + \mathbf{dM}_t$;

`// Endmember update [Mai+10, Algo. 2]`

c — $\mathbf{M}^{(t)} \leftarrow \underset{\mathbf{M} \in \mathcal{M}}{\arg\min}\, \hat{g}_t(\mathbf{M})$;

Result: $\mathbf{M}^{(T)}$, $\{(\mathbf{A}_t, \mathbf{dM}_t)\}_{t=1,\cdots,T}$

Experiments on real data (I)

Data:

- sequence of AVIRIS HS images, acquired of the Mud Lake area (California, USA) between 2014 and 2015;
- 173 exploited bands, outlier corrupted pixels removed from Fig. 9d prior to the unmixing procedure.

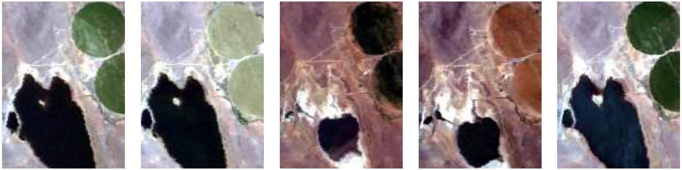

(a) 10/04/14 (b) 02/06/14 (c) 19/09/14 (d) 17/11/14 (e) 29/04/15

Figure 9: Mud Lake dataset.

Remark:

- Sensitivity to outliers $\rightsquigarrow$ robust unmixing of MTHS images (details in the manuscript).

Experiments on real data (II)

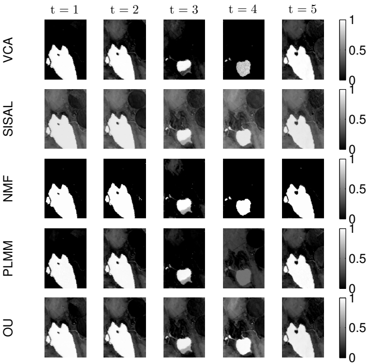

Figure 10: Water abundance maps.

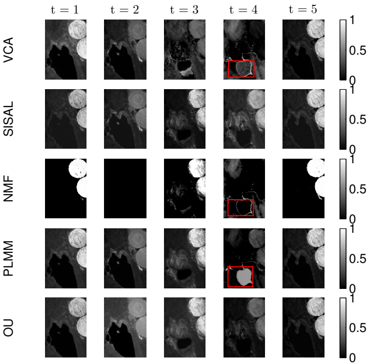

Figure 11: Vegetation abundance maps.

Experiments on real data (III)

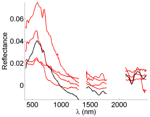

(a) Water (VCA)

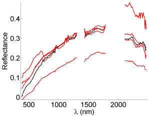

(b) Soil (VCA)

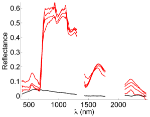

(c) Veg. (VCA)

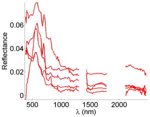

(d) Water (NMF)

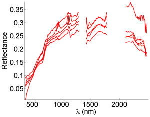

(e) Soil (NMF)

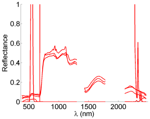

(f) Veg. (NMF)

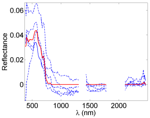

(g) Water (OU)

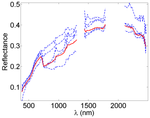

(h) Soil (OU)

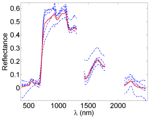

(i) Veg. (OU)

Figure 12: Estimated endmembers (red lines) and their variants affected by variability (blue lines).

Overview

1. A perturbed LMM to account for spatial variability

2. Online unmixing of MTHS images

3. A partially asynchronous distributed unmixing algorithm
   - Motivations
   - Simulations on synthetic data

4. Conclusion and perspectives

Motivations

- Images composed of a possibly large number of pixels $\rightsquigarrow$ use of distributed unmixing procedures
  - ▷ master-slave configuration;

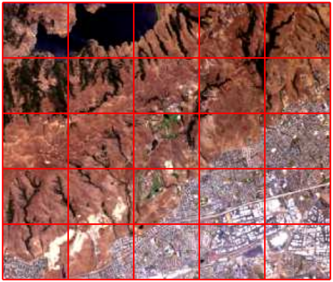

Figure 13: Single HS image divided into sub-images assigned to different nodes.

Motivations

- Images composed of a possibly large number of pixels $\rightsquigarrow$ use of distributed unmixing procedures
  - master-slave configuration;

Figure 13: Sequence of images, each assigned to a computing node.

Motivations

- Images composed of a possibly large number of pixels ⇝ use of distributed unmixing procedures
  - ▷ master-slave configuration;
- Asynchronicity: account for possible discrepancies in the performance of the computational nodes, reduce idle time periods (compared to synchronous algorithms);

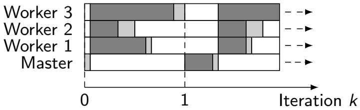

(a) Synchronous system. (b) Asynchronous system.

Figure 13: Illustration of a synchronous and an asynchronous distributed mechanism (idle time in white, transmission delay in light gray, computation delay in gray).

Motivations

- Images composed of a possibly large number of pixels ⇝ use of distributed unmixing procedures
  - ▷ master-slave configuration;
- Asynchronicity: account for possible discrepancies in the performance of the computational nodes, reduce idle time periods (compared to synchronous algorithms);

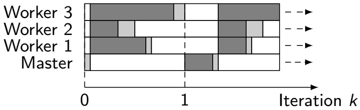

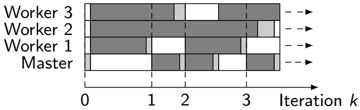

(a) Synchronous system. (b) Asynchronous system.

Figure 13: Illustration of a synchronous and an asynchronous distributed mechanism (idle time in white, transmission delay in light gray, computation delay in gray).

- Significant number of asynchronous algos. recently proposed [CE16; Pen+16a; BJ13; PR15; Sra+16; Li+14; Dav16; Cha+16; FSS15; Pen+16b; Scu+17]
  - ▷ only (a few) synchronous distributed unmixing procedures in the literature [RR13; Sig+16; Sig+17].

Objective

Develop an asynchronous unmixing procedure inspired from the PALM algorithm [BST13; CPR16]

- the standard PALM algorithm easily leads to a synchronous distributed unmixing algorithm
  - $\rightsquigarrow$ reference to assess the interest of the asynchronicity;
- convergence guarantees in the synchronous [BST13; CPR16], and asynchronous case [Can+16].

Problem formulation

Unmixing problem

$$(\mathbf{A}^*, \mathbf{M}^*) \in \arg\min_{\mathbf{A},\mathbf{M}} \Big\{ F(\mathbf{A}, \mathbf{M}) + \alpha\Phi(\mathbf{A}) + \iota_{\mathcal{A}_{R,N}}(\mathbf{A}) + \beta\Psi(\mathbf{M}) + \iota_{\{\cdot \succeq \mathbf{0}\}}(\mathbf{M}) \Big\} \quad \text{with} \tag{14}$$

$$F(\mathbf{A}, \mathbf{M}) = \sum_{i=1}^{I} f_i(\mathbf{M}, \mathbf{A}_i) = \frac{1}{2}\sum_{i=1}^{I} \|\mathbf{Y}_i - \mathbf{M}\mathbf{A}_i\|_{\mathrm{F}}^2$$

$$\mathcal{A}_{R,J} = \Big\{ \mathbf{A} \in \mathbb{R}^{R \times J} : \ \mathbf{a}_n \in \mathcal{S}_R, \ \forall n \in \{1, \cdots, J\} \Big\}$$
$$\mathcal{S}_R = \{ \mathbf{x} \in \mathbb{R}^R : \ x_r \geq 0 \text{ and } \mathbf{x}^\mathsf{T}\mathbf{1}_R = 1 \}$$

- $\iota_{\mathcal{S}}$: indicator function of the set $\mathcal{S}$ ($\iota_{\mathcal{S}} = 0$ if $\mathbf{x} \in \mathcal{S}$, $+\infty$ otherwise)
- Φ et Ψ : appropriate convex penalties
  - in general, Φ is separable to allow a distributed estimation (14);
  - in the following : $\Phi = 0$, Ψ is the mutual distance between the endmembers [Ber+04].

Asynchronous distributed unmixing algorithm (I)

- Each worker updates a subset of the abundance coefficients;
- The master node aggregates the information transmitted by the workers to update the endmembers.

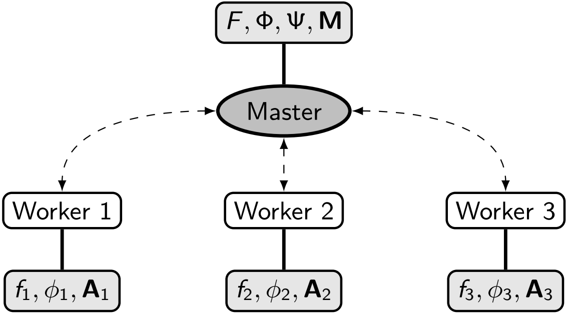

Figure 14: Distribution of the estimation tasks between the computing nodes (for $I = 3$ data blocks).

Asynchronous distributed unmixing algorithm (II)

Algorithm 4: Algorithm of the ith worker.

Data: $\mathbf{M}$, $\tilde{\mathbf{A}}_i$.

begin

Wait for updated endmembers from the master node, $(\mathbf{M}, \tilde{\mathbf{A}}_i)$;

$\hat{\mathbf{A}}_i \in \operatorname{prox}_{\iota_{\mathcal{A}_{R,J}}}\left(\tilde{\mathbf{A}}_i - \frac{1}{c_{\mathbf{A}_i}} \nabla_{\mathbf{A}_i} f_i(\tilde{\mathbf{A}}_i, \mathbf{M})\right)$;

Broadcast $\hat{\mathbf{A}}_i$ to the master node;

Result: $\hat{\mathbf{A}}_i$.

Asynchronous distributed unmixing algorithm (III)

Algorithm 5: Algorithm of the master node.

Data: $\mathbf{A}^0$, $\mathbf{M}^0$, $\mu \in]0,1[$ $(\mu = 10^{-6})$.

$\gamma^0 \leftarrow 1$, $k \leftarrow 0$;

while *stopping criterion not satisfied,* **do**

Wait for $\tilde{\mathbf{A}}_{i^k}$ from one of the workers ;

`// Abundance update`

$$\mathbf{A}_i^{k+1} = \begin{cases} \mathbf{A}_i^k + \gamma^k(\tilde{\mathbf{A}}_i^k - \mathbf{A}_i^k), & i = i^k \\ \mathbf{A}_i^k, & i \neq i^k \end{cases} ;$$

`// Endmember update`

$$\tilde{\mathbf{M}}^k = \mathrm{prox}_{\iota_{\{\cdot \succeq \mathbf{0}\}}}\left(\mathbf{M}^k - \frac{1}{\nu^k}\nabla_{\mathbf{M}}\left[F(\mathbf{A}^{k+1}, \mathbf{M}^k) + \beta\Psi(\mathbf{M}^k)\right]\right);$$

$$\mathbf{M}^{k+1} = \mathbf{M}^k + \gamma^k(\tilde{\mathbf{M}}^k - \mathbf{M}^k);$$

`// Relaxation coefficient update`

$$\gamma^{k+1} = \gamma^k(1 - \mu\gamma^k);$$

`// Broadcast new estimate to the worker` i^k

Broadcast $(\mathbf{M}^{k+1}, \mathbf{A}_{i^k}^{k+1})$ to the worker i^k;

$k \leftarrow k+1$;

Result: $\mathbf{A}^k$, $\mathbf{M}^k$.

Similar algorithm in presence of variability

Distributed unmixing in presence of variability

PLMM

$$\mathbf{y}_n = \sum_{r=1}^{R} (\mathbf{m}_r + \mathbf{dm}_{r,n}) a_{r,n} + \mathbf{b}_n \quad (15)$$

Additional constraints:

$$\|\mathbf{dM}_n\|_F^2 \leq \nu, \text{ where } \mathbf{dM}_n = [\mathbf{dm}_{1,n}, \ldots, \mathbf{dm}_{R,n}] \quad (16)$$

Remarks:

- data distribution similar to the previous case;
- parallel estimation of the abundance coefficients and the variability terms;
- non-negativity constraints on the perturbed endmembers removed (limitation resulting from the asynchronicity).

Simulations on synthetic data (LMM) (I)

- Data : 3 HS images, composed of $R = 9$ endmembers, $L = 413$ spectral bands;
- Images: 100×100 pixels,corrupted by an additive Gaussian noise such that SNR $= 30$ dB;
- Performance evaluation for $I = 3$ processus;
- Initialization: VCA [NB05] / FCLS [HC01];
- Comparison of the algo. with its synchronous counterpart, both implemented in Julia [Bez+17].

Table 1: Simulation results on synthetic data.

	Sync.	Async.
aSAM(**M**) (°)	9.74e-01	1.04e+00
GMSE(**A**)	3.48e-04	5.25e-04
RE	1.05e-04	1.07e-04
aSAM(**Y**) (°)	2.23e-02	2.24e-02
time (s)	1.39e+03	3.33e+02

Simulations on synthetic data (LMM) (II)

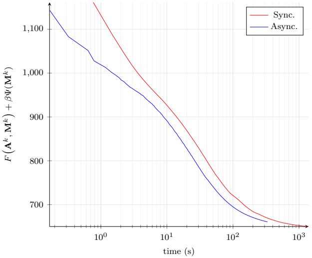

Figure 15: Objective function versus computation time for the synchronous and asynchronous unmixing algorithms (until convergence) [LMM].

Remarks:

- asynchrony promising in terms of computation time (to reach convergence);
- slight performance decrease.

Simulations on synthetic data (PLMM) (I)

- Data: 3 HS images, composed of $R = 3$ endmembers, $L = 413$ spectral bands;
- Images: 100×100 pixels, corrupted by an additive white Gaussian noise such that SNR $= 30$ dB.

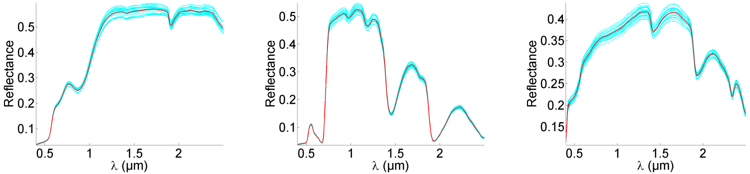

Figure 16: Example of the endmembers (in red) and the corrupted endmembers (in blue) used in the experiments.

Simulations on synthetic data (PLMM) (II)

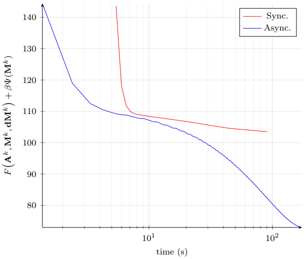

Figure 17: Objective function versus computation time for the synchronous and asynchronous unmixing algorithms (until convergence) [PLMM].

Remarks:

- the results between the synchronous and asynchronous algorithm can differ significantly;
- the asynchronous procedure can converge to a less interesting stationary point than its synchronous counterpart (main limitation).

Overview

Conclusion

Variability modeling:

- Introduction of an explicit mixture model inspired from the total least squares problem, referred to as PLMM
  - represents variability within a single HS image;
  - spatially/spectrally characterizes the observed variability;
  - deterministic counterpart of the NCM [Ech+10].

Conclusion

Variability modeling:

- Introduction of an explicit mixture model inspired from the total least squares problem, referred to as PLMM
  - represents variability within a single HS image;
  - spatially/spectrally characterizes the observed variability;
  - deterministic counterpart of the NCM [Ech+10].
- Robust variant of the PLMM to represent temporal endmember variability and outliers (in the manuscript)
  - represents abrupt and smooth spectral variations occurring over time (information redundancy);
  - model developed within a Bayesian framework.

Conclusion

Variability modeling:

- Introduction of an explicit mixture model inspired from the total least squares problem, referred to as PLMM
  - represents variability within a single HS image;
  - spatially/spectrally characterizes the observed variability;
  - deterministic counterpart of the NCM [Ech+10].
- Robust variant of the PLMM to represent temporal endmember variability and outliers (in the manuscript)
  - represents abrupt and smooth spectral variations occurring over time (information redundancy);
  - model developed within a Bayesian framework.

Computational considerations:

- Study of an online unmixing algorithm to analyze multi-temporal HS images
  - exploits information redundancy between consecutive images;
  - compromise between computational cost and accuracy.

Conclusion

Variability modeling:

- Introduction of an explicit mixture model inspired from the total least squares problem, referred to as PLMM
  - represents variability within a single HS image;
  - spatially/spectrally characterizes the observed variability;
  - deterministic counterpart of the NCM [Ech+10].
- Robust variant of the PLMM to represent temporal endmember variability and outliers (in the manuscript)
  - represents abrupt and smooth spectral variations occurring over time (information redundancy);
  - model developed within a Bayesian framework.

Computational considerations:

- Study of an online unmixing algorithm to analyze multi-temporal HS images
  - exploits information redundancy between consecutive images;
  - compromise between computational cost and accuracy.
- Preliminary study of an asynchronous distributed unmixing algorithm
  - interest and limitations when compared to a synchronous version of the same algorithm.

Perspectives

- **Variability modeling**
  - physically inspired models preserving a distinction between variability modalities (non-linearities, illumination variations, ...);
  - promote different structures for the variability term;
  - estimation of the endmember number in presence of variability.

Perspectives

- **Variability modeling**
  - ▷ physically inspired models preserving a distinction between variability modalities (non-linearities, illumination variations, ...);
  - ▷ promote different structures for the variability term;
  - ▷ estimation of the endmember number in presence of variability.
- **Computational considerations**
  - ▷ automatic hyperparameter selection [Ste81; Del+14];
  - ▷ incorporate variable metrics into the proximal algorithms considered [CPR16; FGP15];
  - ▷ relaxation to the Ising field considered in the robust unmixing

    $\rightsquigarrow$ leverage online estimation techniques.

Perspectives

- **Variability modeling**
  - ▷ physically inspired models preserving a distinction between variability modalities (non-linearities, illumination variations, ...);
  - ▷ promote different structures for the variability term;
  - ▷ estimation of the endmember number in presence of variability.
- **Computational considerations**
  - ▷ automatic hyperparameter selection [Ste81; Del+14];
  - ▷ incorporate variable metrics into the proximal algorithms considered [CPR16; FGP15];
  - ▷ relaxation to the Ising field considered in the robust unmixing
    - $\rightsquigarrow$ leverage online estimation techniques.
- **Application oriented developments**
  - ▷ application to different context: medical imagery [Cav+17], astronomy [Rap+14; CB17];
  - ▷ performance assessment for change detection, with possibly different imaging modalities [Pre+16; YZP17; Fer+17], data fusion [Wei+16].

Thank you for your attention.

Modeling spatial and temporal variabilities in hyperspectral image unmixing

Pierre-Antoine THOUVENIN
PhD defense, IRIT/INP-ENSEEIHT, Toulouse

Supervisor	Nicolas DOBIGEON	Professor at IRIT/INP-ENSEEIHT, Toulouse
Co-supervisor	Jean-Yves TOURNERET	Professor at IRIT/INP-ENSEEIHT, Toulouse
DGA contact	Véronique SERFATY	

University of Toulouse, IRIT/INP-ENSEEIHT

October 17, 2017

Backup slides

- Link between the PLMM and methods from the literature link
- Synthetic variability generation link
- PLMM: experiments on synthetic data link
- Online unmixing: experiments on synthetic data link
- Endmember number: geometrical illustration link
- Robust unmixing of multi-temporal HS images link
- References link
- List of publications link

Link between the PLMM and models from the literature

Back to main slide

The PLMM can be compared with two models from the literature:

- the Generalized NCM (GNCM) [HDT15]
  - the two models are equivalent when considering $\mathbf{m}_{r,n} = \mathbf{m}_r + \mathbf{dm}_{r,n}$;
  - distinction in terms of the adopted estimation approach

$$\mathbf{y}_n = \sum_{r=1}^{R} a_{r,n}\mathbf{m}_{r,n} + \mathbf{b}_n, \qquad \mathbf{m}_{r,n} \sim \mathcal{N}(\mathbf{m}_r, \operatorname{diag}(\boldsymbol{\sigma}_r^2)), \quad \mathbf{b}_n \sim \mathcal{N}(\mathbf{0}_L, \psi_n^2\mathbf{I}_L). \tag{17}$$

Link between the PLMM and models from the literature

The PLMM can be compared with two models from the literature:

- the Generalized NCM (GNCM) [HDT15]
  - ▷ the two models are equivalent when considering $\mathbf{m}_{r,n} = \mathbf{m}_r + \mathbf{dm}_{r,n}$;
  - ▷ distinction in terms of the adopted estimation approach

$$\begin{aligned} \mathbf{y}_n &= \sum_{r=1}^{R} a_{r,n} \mathbf{m}_{r,n} + \mathbf{b}_n, \\ \mathbf{m}_{r,n} &\sim \mathcal{N}(\mathbf{m}_r, \text{diag}(\boldsymbol{\sigma}_r^2)), \quad \mathbf{b}_n \sim \mathcal{N}(\mathbf{0}_L, \psi_n^2 \mathbf{I}_L). \end{aligned} \tag{17}$$

- the Extended LMM (ELMM) [Dru+16] (explicit variability model)
  - ▷ variability represented in terms of spatially varying scaling factors ψ_n;
  - ▷ the scaling indeterminacy introduced ψ_n is partly addressed in the estimation algorithm proposed in [Dru+16]

$$\mathbf{y}_n = \psi_n \sum_{r=1}^{R} a_{r,n} \mathbf{m}_r + \mathbf{b}_n. \tag{18}$$

Variability generation:

- term-wise product of reference endmembers with randomly generated affine functions
  - ▷ spatially varying signatures.

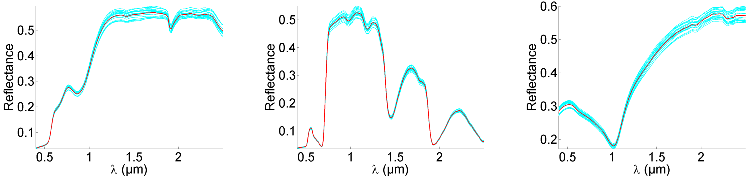

Figure 18: Reference endmembers (red lines) and 20 corresponding instances under spectral variability (cyan lines) involved in the synthetic data experiments.

Experiments on synthetic data [PLMM] (I)

- Data: 128×64 HS images, composed of $R \in \{3, 6\}$ endmembers, with $L = 413$ bands;
- Additive white Gaussian noise: $\mathrm{SNR} = 30\,\mathrm{dB}$;
- Variability generation: term-wise product of reference endmembers with randomly generated affine functions
  - ▷ spatially varying signatures.

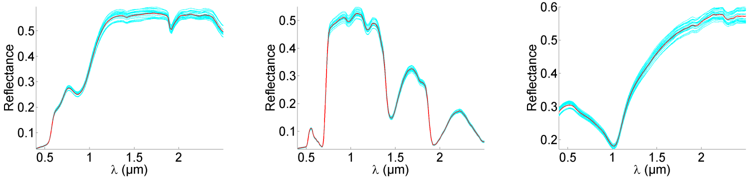

Figure 19: Reference endmembers (red lines) and 20 corresponding instances under spectral variability (cyan lines) involved in the synthetic data experiments.

Experiments on synthetic data [PLMM] (II)

Table 2: Simulation results on synthetic data **in absence of pure pixels** (GMSE($\mathbf{A}$)$\times 10^{-2}$, GMSE($\mathbf{dM}$)$\times 10^{-4}$, RE $\times 10^{-4}$) $[(\alpha, \beta) = (2.1 \times 10^{-1}, 7.7 \times 10^{-6})$ for $R = 3$, $(\alpha, \beta) = (7.1 \times 10^{-1}, 4.3 \times 10^{-6})$ for $R = 6]$.

		aSAM($\mathbf{M}$) (°)	GMSE($\mathbf{A}$)	GMSE($\mathbf{dM}$)	RE	time (s)
$R = 3$	VCA/FCLS	5.06	2.07	/	2.66	**1**
	SISAL/FCLS	4.43	2.16	/	2.56	2
	FDNS	5.06	2.06	/	2.66	3
	AEB	5.11	2.11	/	2.66	33
	ELMM	5.05	1.78	6.86	4.34	329
	ssmdBCD/ADMM ($\gamma = 10^{-1}$)	4.56	**1.49**	6.21	**0.08**	285
	ssmdPALM ($\nu = 5 \times 10^{-2}$)	**4.51**	1.54	**5.24**	0.60	314
$R = 6$	VCA/FCLS	6.55	2.52	/	2.82	**4**
	SISAL/FCLS	6.04	**1.63**	/	2.02	5
	FDNS	6.55	2.53	/	2.82	7
	AEB	**6.00**	1.78	/	1.85	208
	ELMM	6.54	1.98	4.13	**0.60**	555
	ssmdBCD/ADMM ($\gamma = 1$)	6.19	2.19	2.89	0.81	618
	ssmdPALM ($\nu = 2 \times 10^{-1}$)	6.05	2.21	**2.73**	1.82	449

Experiments on synthetic data [PLMM] (III)

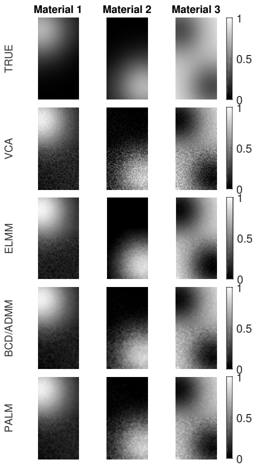

Figure 20: Estimated abundance maps obtained from the synthetic dataset in absence of pure pixels composed of $R = 3$ endmembers.

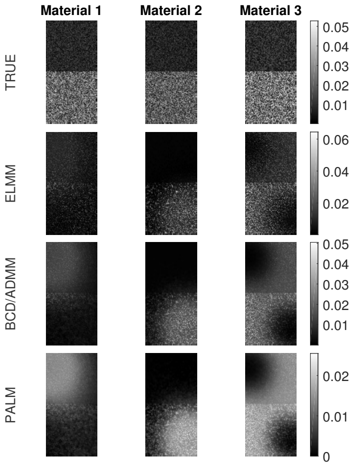

Figure 21: Spatial distribution of the estimated variability w.r.t. each endmember, presented in terms of its energy ($\|\mathbf{dm}_{r,n}\|_2/\sqrt{L}$ for the rth endmember in the nth pixel).

Data:

- sequences of 10 HS images of size 98 × 102, composed of 173 spectral bands;
- endmembers affected by smoothly varying endmember variability, smoothly evolving abundance maps;
- data corrupted by an additive white Gaussian, SNR = 30 dB.

Table 3: Simulation results on synthetic data (GMSE(**A**)$\times 10^{-2}$, GMSE(**dM**)$\times 10^{-4}$, RE $\times 10^{-4}$).

		aSAM(**M**) (°)	GMSE(**A**)	GMSE(**dM**)	RE	aSAM(**Y**) (°)	time (s)
$R=3$	VCA	16.8	4.20	/	0.37	2.81	1.4
	SISAL	16.5	3.83	/	0.35	2.75	3
	$\ell_{1/2}$ NMF	19.4	7.39	/	0.77	3.1	189
	PLMM	17.2	4.22	**0.65**	**0.12**	**1.53**	380
	OU	4.70	0.27	2.07	0.34	2.75	156
	PALM	5.02	**9.67**$\times 10^{-3}$	1.81	0.34	2.75	37
	DSU [HCJ16]	**2.87**	0.35	1.74	3.57	2.76	24

Figure 22: Abundance maps of the first endmember used in the synthetic mixtures. The top line indicates the theoretical maximum abundance value and the true number of pixels whose abundance is greater than 0.95 for each time instant.

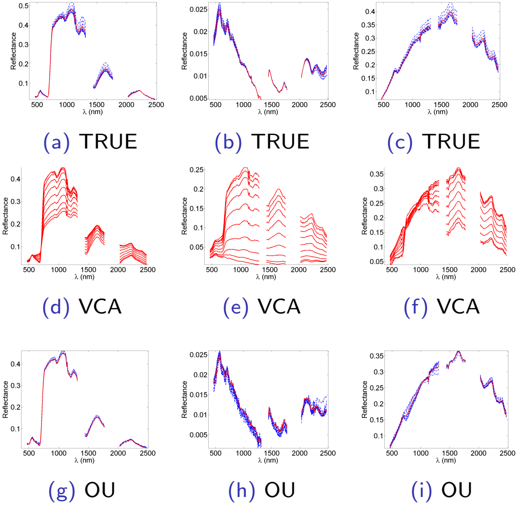

Figure 23: Estimated endmembers from the synthetic hyperspectral time series (extracted endmembers are represented in red, variability in blue dotted lines).

Endmember number: a geometrical illustration

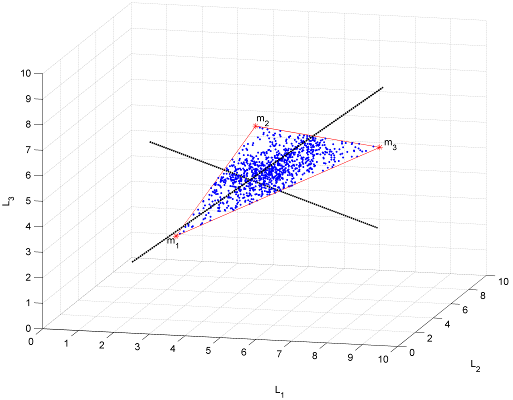

Figure 24: Data projected on the $R - 1$ simplex containing the data (linear model) (image taken from [Dob+09]).

Observations:

- some of the observed materials present moderate variations across time (man-made constructions, ...);

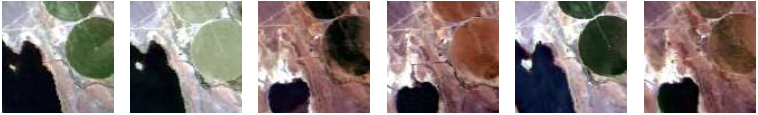

(a) 10/04/14 (b) 02/06/14 (c) 19/09/14 (d) 17/11/14 (e) 29/04/15 (f) 16/10/15

Figure 25: An example of a sequence of hyperspectral images, acquired over the same area at different time instants.

Context and motivations

Back to main slide

Observations:

- some of the observed materials present moderate variations across time (man-made constructions, ...);
- signatures corresponding to materials present in the different images
  - ▷ realizations of reference endmembers $\rightsquigarrow$ variability;

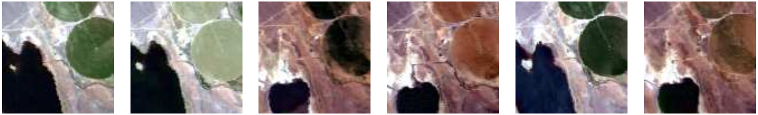

(a) 10/04/14 (b) 02/06/14 (c) 19/09/14 (d) 17/11/14 (e) 29/04/15 (f) 16/10/15

Figure 25: An example of a sequence of hyperspectral images, acquired over the same area at different time instants.

Observations:

- some of the observed materials present moderate variations across time (man-made constructions, ...);
- signatures corresponding to materials present in the different images
  - ▷ realizations of reference endmembers ⇝ variability;
- abrupt variations may occur (e.g., when water or vegetation are present in the observed scene)
  - ▷ new material or a sensor default ⇝ abrupt spectral changes ⇝ outlier w.r.t. the commonly shared materials.

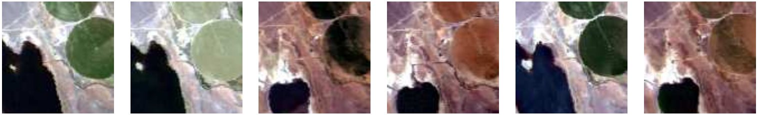

(a) 10/04/14 (b) 02/06/14 (c) 19/09/14 (d) 17/11/14 (e) 29/04/15 (f) 16/10/15

Figure 25: An example of a sequence of hyperspectral images, acquired over the same area at different time instants.

Proposed approach:

- unmix a reference HS image to obtain an initial estimate for the endmembers;
- use / refine this result when unmixing the remaining images.

Model:

- represent smooth endmember variations as temporal variability;
- interpret abrupt spectral variations in terms of outliers.

Model

Model and constraints

$$\mathbf{Y}_t = (\mathbf{M} + \mathbf{dM}_t)\mathbf{A}_t + \mathbf{X}_t + \mathbf{B}_t \tag{19}$$

$$\begin{aligned} &\mathbf{A}_t \succeq \mathbf{0}_{R,N},\ \mathbf{A}_t^\top \mathbf{1}_R = \mathbf{1}_N,\ \forall t \in \{1, \dots, T\} \\ &\mathbf{M} \succeq \mathbf{0}_{L,R},\ \mathbf{M} + \mathbf{dM}_t \succeq \mathbf{0}_{L,R},\ \mathbf{X}_t \succeq \mathbf{0}_{L,N} \end{aligned} \tag{20}$$

Likelihood function

$$p(\underline{\mathbf{Y}} \mid \Theta) \propto \prod_{t=1}^{T} (\sigma_t^2)^{-NL/2} \exp\left(-\frac{1}{2\sigma_t^2} \left\|\mathbf{Y}_t - (\mathbf{M} + \mathbf{dM}_t)\mathbf{A}_t - \mathbf{X}_t\right\|_F^2\right)$$

where $\Theta = \{\mathbf{M}, \mathbf{d}\underline{\mathbf{M}}, \underline{\mathbf{A}}, \underline{\mathbf{X}}, \boldsymbol{\sigma}^2\}$

Objective: infer Θ from $\underline{\mathbf{Y}}$ using $p(\Theta \mid \underline{\mathbf{Y}})$

$\rightsquigarrow$ need for priors on the different parameters/hyperparameters involved in the model.

Parameter estimation: MCMC algorithm (Gibbs sampler) used to build estimators of the parameters of interest.

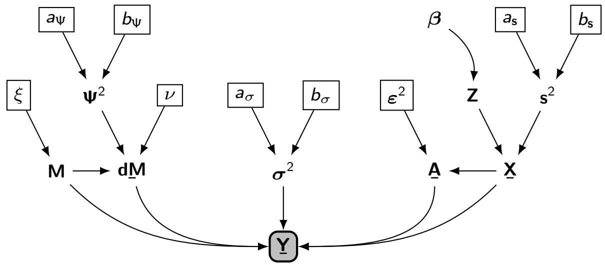

Figure 26: Description of the proposed Bayesian model using a directed acyclic graph (fixed parameters appear in boxes).

Hierachical Bayesian model: priors (I)

Abundance prior

- promotes smooth abundance variations (except when the corresponding pixel contains outliers)
- abundance sum-to-one constraint relaxed ($\mathbf{a}_{n,t}^{\mathsf{T}}\mathbf{1}_R \leq 1$) when outliers are present in the pixel (n, t) (apparition of new materials)

$$\begin{aligned}
\mathbf{a}_{n,1} \mid \mathbf{x}_{n,t} = \mathbf{0}_L &\sim \mathcal{U}_{\mathcal{S}_R} \\
\mathbf{a}_{n,t} \mid \mathbf{x}_{n,t} \neq \mathbf{0}_L &\sim \mathcal{U}_{\widetilde{\mathcal{S}_R}}, \text{ for } t = 1, \dots, T
\end{aligned}$$

$$p\left(\mathbf{a}_{n,t} \mid \mathbf{x}_{n,t} = \mathbf{0}_L, \underline{\mathbf{A}}_{\backslash\{\mathbf{a}_{n,t}\}}\right) \propto \exp\left\{-\frac{1}{2\varepsilon_n^2}\left([\mathscr{T}_{n,t}^1 \neq \emptyset] \left\| a_{n,t} - a_{n,\tau_{n,t}^1} \right\|_2^2\right)\right\} \mathbb{1}_{\mathcal{S}_R}(\mathbf{a}_{n,t}), \text{ for } t \geq 2$$

with

$$\begin{aligned}
\mathcal{S}_R &= \{\mathbf{x} \in \mathbb{R}^R \mid \forall i, x_i \geq 0 \text{ and } \mathbf{x}^{\mathsf{T}}\mathbf{1}_R = 1\} \\
\widetilde{\mathcal{S}_R} &= \{\mathbf{x} \in \mathbb{R}^R \mid \forall i, x_i \geq 0 \text{ and } \mathbf{x}^{\mathsf{T}}\mathbf{1}_R \leq 1\} \\
\mathscr{T}_{n,t}^1 &= \{\tau < t \mid \mathbf{x}_{n,\tau} = \mathbf{0}\}, \quad \tau_{n,t}^1 = \max_{\tau \in \mathscr{T}_{n,t}^1} \tau.
\end{aligned}$$

Hierachical Bayesian model: priors (II)

Outlier prior

- promotes outlier sparsity [KM82; Lav93; BC05; BDT11; VS13];
- takes advantage of possible spatial correlations between these outliers by modeling $\mathbf{z}_t \in \mathbb{R}^N$ as Ising-Markov random fields (correlations likely to occur when new materials appear)

$$p(\mathbf{x}_{n,t} \mid z_{n,t}, s_t^2) = (1 - z_{n,t})\delta(\mathbf{x}_{n,t}) + z_{n,t}\mathcal{N}_{\mathbb{R}_+^L}(\mathbf{0}_L, s_t^2).$$

Hierachical Bayesian model: priors (II)

Outlier prior

- promotes outlier sparsity [KM82; Lav93; BC05; BDT11; VS13];
- takes advantage of possible spatial correlations between these outliers by modeling $\mathbf{z}_t \in \mathbb{R}^N$ as Ising-Markov random fields (correlations likely to occur when new materials appear)

$$p(\mathbf{x}_{n,t} \mid z_{n,t}, s_t^2) = (1 - z_{n,t})\delta(\mathbf{x}_{n,t}) + z_{n,t}\mathcal{N}_{\mathbb{R}_+^L}(\mathbf{0}_L, s_t^2).$$

Variability prior

- promotes smooth endmember variations from an image to another [Hal+15; HCJ16]

$$dm_{\ell,r,1} \mid m_{\ell,r} \sim \mathcal{N}_{\mathcal{I}_{\ell,r}}(0, \nu),\ \mathcal{I}_{\ell,r} = [-m_{\ell,r}, +\infty)$$

$$dm_{\ell,r,t} | m_{\ell,r}, dm_{\ell,r,(t-1)}, \psi_{\ell,r}^2 \sim \mathcal{N}_{\mathcal{I}_{\ell,r}}\left(dm_{\ell,r,(t-1)}, \psi_{\ell,r}^2\right)$$

- ν penalizes the variability energy in the first image;
- $\psi_{\ell,r}^2$ controls the temporal evolution of the variability.

Priors assigned to the remaining parameters

Endmember prior

- endmembers can be *a priori* considered to live in a subspace of dimension $K \ll L$ (PCA or rPCA [Can+09]);
- considering the decomposition used in [Dob+09] leads to

$$\mathbf{m}_r = (\mathbf{I}_L - \mathbf{U}\mathbf{U}^\mathsf{T})\bar{\mathbf{y}} + \mathbf{U}\mathbf{e}_r, \quad \mathbf{U}^\mathsf{T}\mathbf{U} = \mathbf{I}_K$$

  where $\mathbf{U}$ is a basis of the subspace and $\bar{\mathbf{y}}$ is the sample mean of $\underline{\mathbf{Y}}$;
- projected endmembers $\mathbf{e}_r$ are assigned a truncated multivariate Gaussian prior to ensure the non-negativity of $\mathbf{m}_r$

$$\mathbf{e}_r \sim \mathcal{N}_{\mathcal{E}_r}(\mathbf{0}_K, \xi\mathbf{I}_K), \text{ for } r = 1, \ldots, R. \tag{21}$$

Hyperparameter priors

- conjugate inverse-gamma priors assigned to the noise ($\boldsymbol{\sigma}^2$), the variability ($\boldsymbol{\Psi}^2$) and the outlier ($\mathbf{s}^2$) variances, i.e.,

$$\sigma_t^2 \sim \mathcal{IG}(a_\sigma, b_\sigma),\ \psi_{\ell,r}^2 \sim \mathcal{IG}(a_\Psi, b_\Psi),\ s_t^2 \sim \mathcal{IG}(a_\mathbf{s}, b_\mathbf{s}) \tag{22}$$

where $a_\sigma = b_\sigma = a_\Psi = b_\Psi = a_\mathbf{s} = b_\mathbf{s} = 10^{-3}$.

Algorithm 6: Proposed Gibbs sampler.

Input: N_{bi}, N_{MC}, $\Theta^{(0)}$, $\boldsymbol{\beta}$, ξ, a_Ψ, b_Ψ, $a_{\mathbf{s}}$, $b_{\mathbf{s}}$, a_σ, b_σ, ν, $\boldsymbol{\varepsilon}^2$.

for $q = 1$ **to** N_{MC} **do**

- **for** $(n, t) = (1, 1)$ **to** (N, T) **do**
  - Draw $\mathbf{a}_{n,t}^{(q)} \sim p\big(\mathbf{a}_{n,t} \mid \mathbf{y}_{n,t}, \Theta_{\setminus\{\mathbf{a}_{n,t}\}}\big)$;
- **for** $r = 1$ **to** R **do**
  - Draw $\mathbf{e}_r^{(q)} \sim p\big(\mathbf{e}_r \mid \underline{\mathbf{Y}}, \Theta_{\setminus\{\mathbf{e}_r\}}\big)$;
- **for** $t = 1$ **to** T **do**
  - Draw $\mathbf{dM}_t^{(q)} \sim p\big(\mathbf{dM}_t \mid \mathbf{Y}_t, \Theta_{\setminus\{\mathbf{dM}_t\}}\big)$;
- **for** $(n, t) = (1, 1)$ **to** (N, T) **do**
  - Draw $z_{n,t}^{(q)} \sim \mathbb{P}\big[z_{n,t} \mid \mathbf{y}_{n,t}, \Theta_{\setminus\{z_{n,t}\}}\big]$;
  - Draw $\mathbf{x}_{n,t}^{(q)} \sim p\big(\mathbf{x}_{n,t} \mid \Theta_{\setminus\{\mathbf{x}_{n,t}\}}\big)$;
- **for** $t = 1$ **to** T **do**
  - Draw $s_t^{2(q)} \sim p\big(s_t^2 \mid \Theta_{\setminus\{s_t^2\}}\big)$;
- **for** $t = 1$ **to** T **do**
  - Draw $\sigma_t^{2(q)} \sim p\big(\sigma_t^2 \mid \Theta_{\setminus\{\sigma_t^2\}}\big)$;
- **for** $(\ell, r) = (1, 1)$ **to** (L, R) **do**
  - Draw $\psi_{\ell,r}^{2(q)} \sim p\big(\psi_{\ell,r}^2 \mid \Theta_{\setminus\{\psi_{\ell,r}^2\}}\big)$;
- **for** $t = 1$ **to** T **do**
  - Draw β_t (Metropolis-Hastings step) ;

Experiments on synthetic data (I)

Data generation:

- MTHS image composed of 10 images of size 50×50, $L = 413$ bands, affected by smooth time-varying variability and additive white Gaussian noise;
- mimics the emergence of a previously undetected material in a few pixels within specific images $\rightsquigarrow$ outliers.

Algorithmic setting (synthetic data):

- $\mathbf{X}_t^{(0)} = \mathbf{0}_{L,N}$, $\mathbf{dM}_t^{(0)} = \mathbf{0}_{L,R}$, $z_{n,t}^{(0)} = 0$, $\sigma_t^{2(0)} = 10^{-4}$, $\psi_{\ell,r}^{2(0)} = 10^{-3}$, $s_t^{2(0)} = 5 \times 10^{-3}$, $\beta_t^{(0)} = 1.7$;
- numerical constants: $\varepsilon_n = 10^{-3}$, $\nu = 10^{-3}$;
- $N_{\mathrm{MC}} = 400$ M-C iterations, with $N_{\mathrm{bi}} = 350$ burn-in iterations.

Table 4: Simulation results on synthetic multi-temporal data (GMSE($\mathbf{A}$)$\times 10^{-2}$, GMSE($\mathbf{dM}$)$\times 10^{-4}$, RE $\times 10^{-4}$).

		aSAM(**M**) (°)	GMSE(**A**)	GMSE(**dM**)	RE	time (s)
$R = 3$ (♯1)	VCA/FCLS	6.07	2.32	/	3.91	**1**
	SISAL/FCLS	5.07	1.71	/	2.28	2
	RLMM	5.13	2.04	/	**0.31**	463
	DSU	5.18	0.53	11.5	2.21	8
	OU	**1.90**	0.42	3.22	2.61	98
	Proposed	2.03	**0.15**	**1.85**	2.00	2530

Experiments on synthetic data (II)

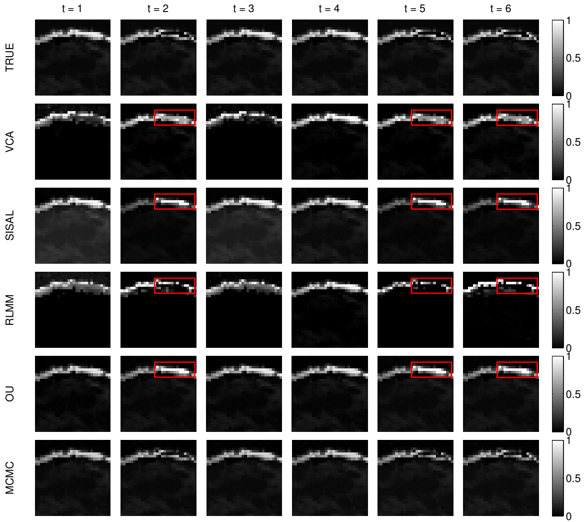

Figure 27: Abundance maps estimated for the third endmember for $t = 1$ to 6. The areas corrupted by outliers are delineated in red.

Experiments on synthetic data (III)

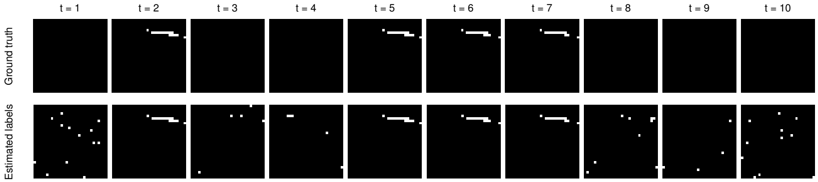

Figure 28: Ground truth (first row) and estimated labels (second row) obtained with the proposed method for $t = 1$ to 10, where each column corresponds to a time instant [0 in black, 1 in white].

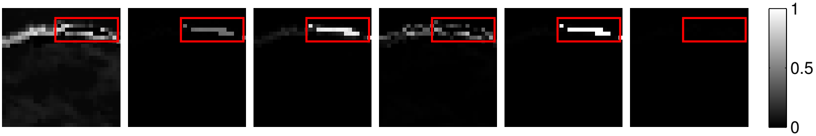

Figure 29: Map of the re-scaled abundance estimation errors for the third endmember at time $t = 2$ (from left to right: true abundances, estimation error of VCA/FCLS, SISAL/FCLS, rLMM, OU and the proposed method). Except for the proposed method, the results exhibit notable errors in pixels corrupted by outliers (area in red).

Experiments on synthetic data (IV)

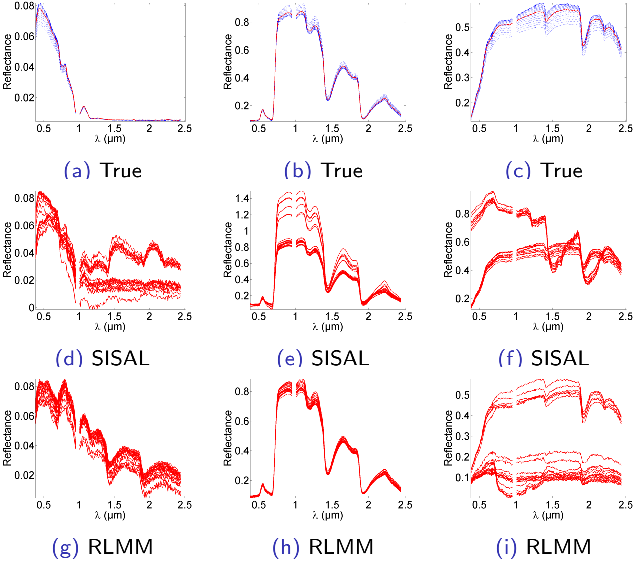

Figure 30: Endmembers (red lines) and corrupted endmembers (blue dotted lines).

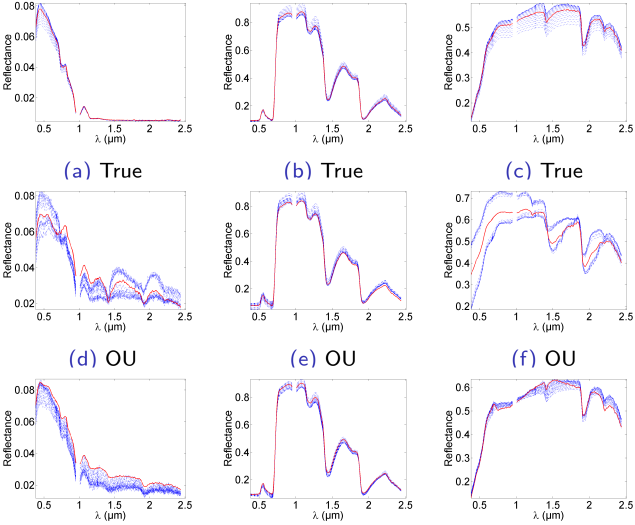

(a) True (b) True (c) True

(d) OU (e) OU (f) OU

(g) MCMC (h) MCMC (i) MCMC

Figure 31: Endmembers (red lines) and corrupted endmembers (blue dotted lines).

Data:

- real sequence of 100 × 100 HS images acquired by the AVIRIS sensor, Mud Lake, California, USA;
- 173 exploited bands, out of the 224 available bands.

(a) 10/04/14 (b) 02/06/14 (c) 19/09/14 (d) 17/11/14 (e) 29/04/15 (f) 16/10/15

Figure 32: Scenes used in the experiment, given with their respective acquisition date. The area delineated in red in Fig. 32e highlights a region known to contain outliers.

Experiments on real data (II)

Back to main slide

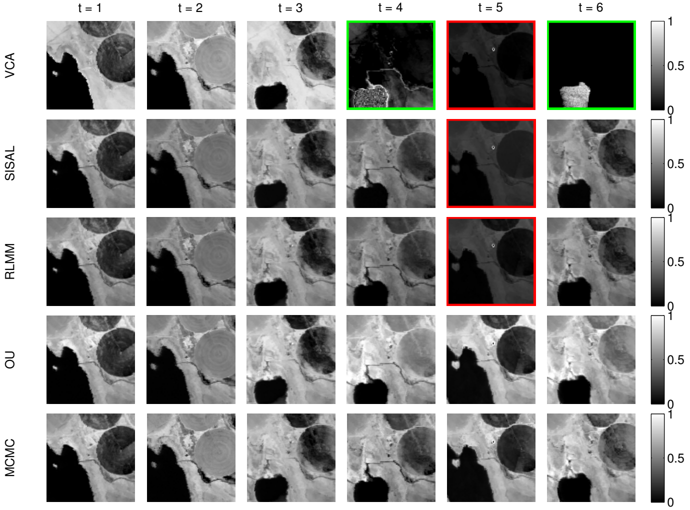

Figure 33: Soil abundance map recovered by the different methods (in row) at each time instant (in column) [VCA/FCLS, SISAL/FCLS, RLMM, OU, MCMC].

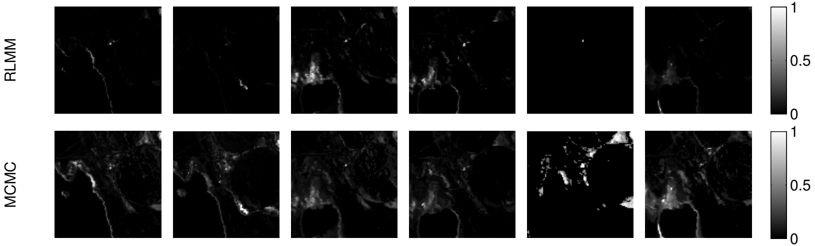

Figure 34: Outlier energy recovered by RLMM [FD15] and the proposed MCMC method.

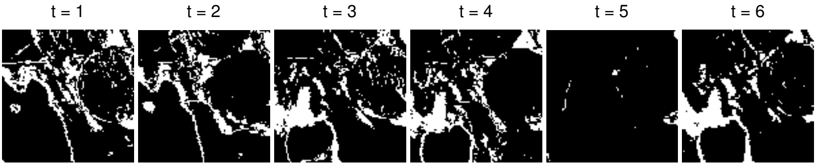

Figure 35: Non-linearity maps estimated by [Alt+13] applied to each image with the SISAL-extracted endmembers.

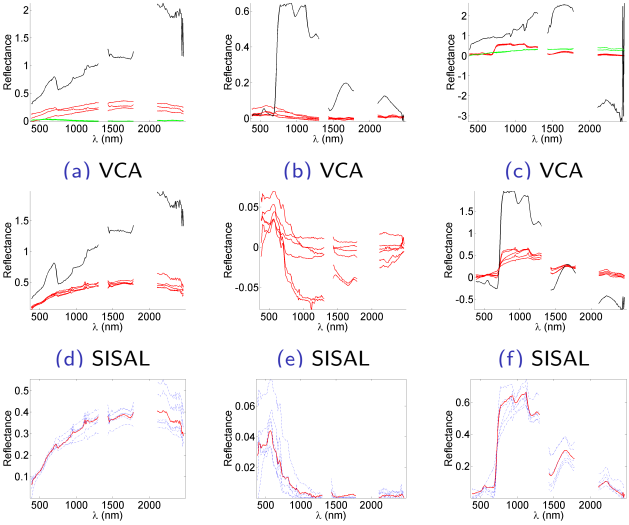

(a) VCA (b) VCA (c) VCA

(d) SISAL (e) SISAL (f) SISAL

(g) MCMC (h) MCMC (i) MCMC

Figure 36: Extracted endmembers (red lines) and perturbed endmembers (blue lines).

References I

[ADT14] Y. Altmann, N. Dobigeon, and J.-Y. Tourneret. "Unsupervised post-nonlinear unmixing of hyperspectral images using a Hamiltonian Monte Carlo algorithm". In: *IEEE Trans. Image Process.* 23.6 (June 2014), pp. 2663–2675 (cit. on p. 6).

[Alt+13] Y. Altmann et al. "A robust test for nonlinear mixture detection in hyperspectral images". In: *Proc. IEEE Int. Conf. Acoust., Speech, and Signal Processing (ICASSP)*. Vancouver, Canada, June 2013, pp. 2149–2153 (cit. on p. 86).

[BC05] S. Bourguignon and H. Carfantan. "Bernoulli-Gaussian spectral analysis of unevenly spaced astrophysical data". In: *Proc. IEEE-SP Workshop Stat. and Signal Processing (SSP)*. Bordeaux, France, July 2005, pp. 811–816 (cit. on pp. 75, 76).

[BDT11] C. Bazot, N. Dobigeon, and J.-Y. Tourneret. "Bernoulli-Gaussian model for gene expression analysis". In: *Proc. IEEE Int. Conf. Acoust., Speech, and Signal Processing (ICASSP)*. Prague, Czech Republic, May 2011, pp. 5996–5999 (cit. on pp. 75, 76).

References II

[Ber+04] M. Berman et al. "ICE: a statistical approach to identifying endmembers in hyperspectral images". In: *IEEE Trans. Geosci. Remote Sens.* 42.10 (Oct. 2004), pp. 2085–2095 (cit. on pp. 16, 38).

[Bez+17] J. Bezanson et al. "Julia: a fresh approach to numerical computing". In: *SIAM Review* 59.1 (2017), pp. 65–98. DOI: 10.1137/141000671 (cit. on p. 43).

[Bio+12] J. M. Bioucas-Dias et al. "Hyperspectral unmixing overview: geometrical, statistical, and sparse regression-based approaches". In: *IEEE J. Sel. Topics Appl. Earth Observ. in Remote Sens.* 5.2 (Apr. 2012), pp. 354–379 (cit. on pp. 4–6).

[BJ13] P. Bianchi and J. Jakubowicz. "Convergence of a multi-agent projected stochastic gradient algorithm for non-convex optimization". In: *IEEE Trans. Autom. Control* 58.2 (Feb. 2013), pp. 391–405 (cit. on pp. 33–36).

References III

[BST13] J. Bolte, S. Sabach, and M. Teboulle. "Proximal alternating linearized minimization for nonconvex and nonsmooth problems". In: *Mathematical Programming* 1-2.146 (July 2013), pp. 459–494 (cit. on pp. 15, 18, 28, 37).

[Can+09] E. J. Candès et al. "Robust principal component analysis?" In: *journaltitle of ACM* 58.1 (2009), pp. 1–37 (cit. on p. 77).

[Can+16] L. Cannelli et al. "Asynchronous Parallel Algorithms for Nonconvex Big-Data Optimization. Part I: Model and Convergence". In: (July 2016). arXiv preprint. URL: https://arxiv.org/abs/1607.04818 (cit. on p. 37).

[Cav+17] Y. C. Cavalcanti et al. "Unmixing dynamic PET images with a PALM algorithm". In: *Proc. European Signal Process. Conf. (EUSIPCO)*. to appear. Kos, Greece, Sept. 2017 (cit. on pp. 52–54).

[CB17] C. Chenot and J. Bobin. "Blind separation of sparse sources in the presence of outliers". In: *Signal Processing* 138 (Sept. 2017), pp. 233–243 (cit. on pp. 52–54).

References IV

[CE16] P. L. Combettes and J. Eckstein. "Asynchronous block-iterative primal-dual decomposition methods for monotone inclusions". In: *Math. Program., Ser. B* (2016), pp. 1–28 (cit. on pp. 33–36).

[Cha+16] T.-H. Chang et al. "Asynchronous Distributed ADMM for Large-Scale Optimization–Part I: Algorithm and Convergence Analysis". In: *IEEE Trans. Signal Process.* 62.12 (June 2016), pp. 3118–3130 (cit. on pp. 33–36).

[CPR16] E. Chouzenoux, J.-C. Pesquet, and A. Repetti. "A block coordinate variable metric forward-backward algorithm". In: *J. Glob. Optim* 66.3 (2016), pp. 547–485 (cit. on pp. 18, 28, 37, 52–54).

[CRH14] J. Chen, C. Richard, and P. Honeine. "Nonlinear estimation of material abundance in hyperspectral images with ℓ_1-norm spatial regularization". In: *IEEE Trans. Geosci. Remote Sens.* 52.5 (May 2014), pp. 2654–2665 (cit. on p. 16).

[Dav16] D. Davis. "The asynchronous PALM algorithm for nonsmooth nonconvex problems". In: (Apr. 2016). submitted. URL: https://arxiv.org/abs/1604.00526 (cit. on pp. 33–36).

References V

[Del+14] C.-A. Deledalle et al. "Stein unbiased gradient estimator of the risk (sugar) for multiple parameter selection". In: *SIAM J. Imaging Sciences* 7.4 (2014), pp. 2448–2487 (cit. on pp. 52–54).

[Dob+09] N. Dobigeon et al. "Joint Bayesian endmember extraction and linear unmixing for hyperspectral imagery". In: *IEEE Trans. Signal Process.* 57.11 (Nov. 2009), pp. 4355–4368 (cit. on pp. 19, 67, 77).

[Dob+14] N. Dobigeon et al. "Nonlinear unmixing of hyperspectral images: models and algorithms". In: *IEEE Signal Process. Mag.* 31.1 (Jan. 2014), pp. 89–94 (cit. on p. 6).

[Dru+16] L. Drumetz et al. "Blind hyperspectral unmixing using an extended linear mixing model to address spectral variability". In: *IEEE Trans. Image Process.* 25.8 (Aug. 2016), pp. 3890–3905 (cit. on pp. 58, 59).

[Du+14] X. Du et al. "Spatial and spectral unmixing using the beta compositional model". In: *IEEE J. Sel. Topics Appl. Earth Observ. in Remote Sens.* 7.6 (June 2014), pp. 1994–2003 (cit. on pp. 9–11).

References VI

[Ech+10] O. Eches et al. "Bayesian estimation of linear mixtures using the normal compositional model. Application to hyperspectral imagery". In: *IEEE Trans. Image Process.* 19.6 (June 2010), pp. 1403–1413 (cit. on pp. 9–11, 48–51).

[EDT11] O. Eches, N. Dobigeon, and J. Y. Tourneret. "Enhancing hyperspectral image unmixing with spatial correlations". In: *IEEE Trans. Geosci. Remote Sens.* 49.11 (Nov. 2011), pp. 4239–4247 (cit. on p. 19).

[FD15] C. Févotte and N. Dobigeon. "Nonlinear hyperspectral unmixing with robust nonnegative matrix factorization". In: *IEEE Trans. Image Process.* 24.12 (Dec. 2015), pp. 4904–4917 (cit. on p. 86).

[Fer+17] V. Ferraris et al. "Robust fusion of multiband images with different spatial and spectral resolutions for change detection". In: *IEEE Trans. Comput. Imag.* 3.2 (June 2017), pp. 175–186 (cit. on pp. 52–54).

References VII

[FGP15] P. Frankel, G. Garrigos, and J. Peypouquet. "Splitting methods with variable metric for Kurdyka-Łojasiewicz functions and general convergence rates". In: *J. Optim. Theory Appl.* 165.1 (2015), pp. 874–900 (cit. on pp. 52–54).

[FSS15] F. Facchinei, G. Scutari, and S. Sagratella. "Parallel selective algorithms for nonconvex big data optimization". In: *IEEE Trans. Signal Process.* 63.7 (Apr. 2015), pp. 1874–1889 (cit. on pp. 33–36).

[Gad+13] P. Gader et al. *MUUFL gulfport hyperspectral and LiDAR airborne data set*. Tech. rep. REP-2013-570. Gainesville, FL: University of Florida, Oct. 2013 (cit. on p. 7).

[Goe+13] M. A. Goenaga et al. "Unmixing analysis of a time series of hyperion images over the Guánica dry forest in Puerto Rico". In: *IEEE J. Sel. Topics Appl. Earth Observ. in Remote Sens.* 6.2 (Apr. 2013), pp. 329–338 (cit. on pp. 9–11).

[Hal+11] A. Halimi et al. "Nonlinear unmixing of hyperspectral images using a generalized bilinear model". In: *IEEE Trans. Geosci. Remote Sens.* 49.11 (Nov. 2011), pp. 4153–4162 (cit. on pp. 6, 19).

References VIII

[Hal+15] A. Halimi et al. "Unmixing hyperspectral images accounting for temporal and spatial endmember variability". In: *Proc. European Signal Process. Conf. (EUSIPCO)*. Nice, France, Sept. 2015, pp. 1686–1690 (cit. on pp. 75, 76).

[HC01] D. C. Heinz and C. -I Chang. "Fully constrained least-squares linear spectral mixture analysis method for material quantification in hyperspectral imagery". In: *IEEE Trans. Geosci. Remote Sens.* 29.3 (Mar. 2001), pp. 529–545 (cit. on p. 43).

[HCJ16] S. Henrot, J. Chanussot, and C. Jutten. "Dynamical spectral unmixing of multitemporal hyperspectral images". In: *IEEE Trans. Image Process.* 25.7 (July 2016), pp. 3219–3232 (cit. on pp. 64, 75, 76).

[HDT15] A. Halimi, N. Dobigeon, and J.-Y. Tourneret. "Unsupervised unmixing of hyperspectral images accounting for endmember variability". In: *IEEE Trans. Image Process.* 24.12 (Dec. 2015), pp. 4904–4917 (cit. on pp. 9–11, 58, 59).

[HPG14] R. Heylen, M. Parente, and P. Gader. "A review of nonlinear hyperspectral unmixing methods". In: *IEEE J. Sel. Topics Appl. Earth Observ. in Remote Sens.* 7.6 (June 2014), pp. 1844–1868 (cit. on p. 6).

[KM82] J. J. Kormylo and J. M. Mendel. "Maximum likelihood detection and estimation of Bernoulli-Gaussian processes". In: *IEEE Trans. Inf. Theory* 28.3 (May 1982), pp. 482–488 (cit. on pp. 75, 76).

[Lav93] M. Lavielle. "Bayesian deconvolution of Bernoulli-Gaussian processes". In: *Signal Process.* 33.1 (July 1993), pp. 67–79 (cit. on pp. 75, 76).

[Li+14] M. Li et al. "Communication efficient distributed machine learning with the parameter server". In: *Adv. in Neural Information Processing Systems*. 2014, pp. 91–27 (cit. on pp. 33–36).

[Mai+10] J. Mairal et al. "Online learning for matrix factorization and sparse coding". In: *J. Mach. Learning Research* 11 (Jan. 2010), pp. 19–60 (cit. on pp. 26, 28).

References X

[NB05] J. M. Nascimento and J. M. Bioucas-Dias. "Vertex component analysis: a fast algorithm to unmix hyperspectral data". In: *IEEE Trans. Geosci. Remote Sens.* 43.4 (Apr. 2005), pp. 898–910 (cit. on p. 43).

[Pen+16a] Z. Peng et al. "Arock: an algorithmic framework for asynchronous parallel coordinate updates". In: *SIAM J. Sci. Comput.* 38.5 (Sept. 2016), pp. 2851–2879 (cit. on pp. 33–36).

[Pen+16b] Z. Peng et al. "On the convergence of asynchronous parallel iteration with arbitrary delays". In: (Dec. 2016). arXiv preprint. URL: https://arxiv.org/abs/1612.04425 (cit. on pp. 33–36).

[PR15] J.-C. Pesquet and A. Repetti. "A Class of Randomized Primal-Dual Algorithms for Distributed Optimization". In: *Journal of nonlinear and convex analysis* 16.12 (Nov. 2015), pp. 2453–2490 (cit. on pp. 33–36).

[Pre+16] J. Prendes et al. "A Bayesian Nonparametric Model Coupled with a Markov Random Field for Change Detection in Heterogeneous Remote Sensing Images". In: *SIAM J. Imaging Sciences* 9.4 (2016), pp. 1889–1921 (cit. on pp. 52–54).

References XI

[Rap+14] J. Rapin et al. "NMF with sparse regularizations in transformed domains". In: *SIAM J. Imaging Sciences* 7.4 (2014), pp. 2020–2047 (cit. on pp. 52–54).

[Rob+98] D. Roberts et al. "Mapping chaparral in the Santa Monica mountain using multiple endmember spectral mixture models". In: *Remote Sens. Environment* 65.3 (Sept. 1998), pp. 267–279 (cit. on pp. 9–11).

[RR13] S. A. Robila and D. Ricart. "Distributed algorithms for unmixing hyperspectral data using nonnegative matrix factorization with sparsity constraints". In: *Proc. IEEE Int. Conf. Geosci. Remote Sens. (IGARSS)*. Melbourne, Australia, July 2013, pp. 2156–2159 (cit. on pp. 33–36).

[RX11] D. Ralph and H. Xu. "Convergence of stationary points of sample average two-stage stochastic programs: a generalized equation approach". In: *Mathematics of Operations Research* 36.3 (Aug. 2011), pp. 568–592 (cit. on p. 27).

References XII

[Scu+17] G. Scutari et al. "Parallel and distributed methods for nonconvex optimization-part i: theory". In: *IEEE Trans. Signal Process.* 65.8 (Apr. 2017), pp. 1929–2944 (cit. on pp. 33–36).

[Sig+16] J. Sigurdsson et al. "Sparse distributed hyperspectral unmixing". In: *Proc. IEEE Int. Conf. Geosci. Remote Sens. (IGARSS)*. Beijing, China, July 2016, pp. 6994–6997 (cit. on pp. 33–36).

[Sig+17] J. Sigurdsson et al. "Sparse distributed multitemporal hyperspectral unmixing". In: *IEEE Trans. Geosci. Remote Sens.* (2017). accepted (cit. on pp. 33–36).

[Som+12] B. Somers et al. "Automated extraction of image-based endmember bundles for improved spectral unmixing". In: *IEEE J. Sel. Topics Appl. Earth Observ. in Remote Sens.* 5.2 (Apr. 2012), pp. 396–408 (cit. on pp. 9–11).

[Sra+16] S. Sra et al. "Adadelay: delay adaptive distributed stochastic optimization". In: *Proc. Int. Conf. Artificial Intelligence and Statistics (AISTATS)*. 16. Cadiz, Spain, 2016, pp. 957–965 (cit. on pp. 33–36).

References XIII

[Ste81] C. M. Stein. "Estimation of the mean of a multivariate normal distribution". In: *The Annals of Statistics* 9.6 (Nov. 1981), pp. 1135–1151 (cit. on pp. 52–54).

[TDT15a] P.-A. Thouvenin, N. Dobigeon, and J.-Y. Tourneret. "A perturbed linear mixing model accounting for spectral variability". In: *Proc. European Signal Process. Conf. (EUSIPCO)*. Nice, France, Sept. 2015, pp. 819–823.

[TDT15b] P.-A. Thouvenin, N. Dobigeon, and J.-Y. Tourneret. "Estimation de variabilité pour le démélange non-supervisé d'images hyperspectrales". In: *Actes du XXVième Colloque GRETSI*. in French. Lyon, France, Sept. 2015.

[TDT16a] P.-A. Thouvenin, N. Dobigeon, and J.-Y. Tourneret. "Hyperspectral unmixing with spectral variability using a perturbed linear mixing model". In: *IEEE Trans. Signal Process.* 64.2 (Jan. 2016), pp. 525–538.

[TDT16b] P.-A. Thouvenin, N. Dobigeon, and J.-Y. Tourneret. "Online unmixing of multitemporal hyperspectral images accounting for spectral variability". In: *IEEE Trans. Image Process.* 25.9 (Sept. 2016), pp. 3979–3990.

[TDT16c] P.-A. Thouvenin, N. Dobigeon, and J.-Y. Tourneret. "Unmixing multitemporal hyperspectral images with variability: an online algorithm". In: *Proc. IEEE Int. Conf. Acoust., Speech, and Signal Processing (ICASSP)*. Shanghai, China, Mar. 2016, pp. 3351–3355.

[TDT17a] P.-A. Thouvenin, N. Dobigeon, and J.-Y. Tourneret. "Une approche distribuée asynchrone pour la factorisation en matrices non-négatives – application au démélange hyperspectral". In: *Actes du XXVIième Colloque GRETSI*. in French. Juan-les-Pins, France, Sept. 2017.

[TDT17b] P.-A. Thouvenin, N. Dobigeon, and J.-Y. Tourneret. "Unmixing Multitemporal Hyperspectral Images Accounting for Smooth and Abrupt Variations". In: *Proc. European Signal Process. Conf. (EUSIPCO)*. Kos, Greece, Sept. 2017, pp. 2442–2446.

[VS13] J. P. Vila and P. Schniter. "Expectation-Maximization Gaussian-mixture approximate message passing". In: *IEEE Trans. Signal Process.* 61.19 (Oct. 2013), pp. 4658–4672 (cit. on pp. 75, 76).

[Wei+16] Q. Wei et al. "Multiband image fusion based on spectral unmixing". In: *IEEE Trans. Geosci. Remote Sens.* 54.12 (Dec. 2016), pp. 7236–7249 (cit. on pp. 52–54).

[YZP17] N. Yokoya, X. X. Zhu, and A. Plaza. "Multisensor Coupled Spectral Unmixing for Time-Series Analysis". In: *IEEE Trans. Geosci. Remote Sens.* 55.5 (May 2017), pp. 2842–2857 (cit. on pp. 52–54).

Back to main slide

International journals

[TDT16a] P.-A. Thouvenin, N. Dobigeon, and J.-Y. Tourneret. "Hyperspectral unmixing with spectral variability using a perturbed linear mixing model". In: *IEEE Trans. Signal Process.* 64.2 (Jan. 2016), pp. 525–538.

[TDT16b] P.-A. Thouvenin, N. Dobigeon, and J.-Y. Tourneret. "Online unmixing of multitemporal hyperspectral images accounting for spectral variability". In: *IEEE Trans. Image Process.* 25.9 (Sept. 2016), pp. 3979–3990.

International conferences

[TDT15a] P.-A. Thouvenin, N. Dobigeon, and J.-Y. Tourneret. "A perturbed linear mixing model accounting for spectral variability". In: *Proc. European Signal Process. Conf. (EUSIPCO)*. Nice, France, Sept. 2015, pp. 819–823.

List of publications II

[TDT16c] P.-A. Thouvenin, N. Dobigeon, and J.-Y. Tourneret. "Unmixing multitemporal hyperspectral images with variability: an online algorithm". In: *Proc. IEEE Int. Conf. Acoust., Speech, and Signal Processing (ICASSP)*. Shanghai, China, Mar. 2016, pp. 3351–3355.

[TDT17b] P.-A. Thouvenin, N. Dobigeon, and J.-Y. Tourneret. "Unmixing Multitemporal Hyperspectral Images Accounting for Smooth and Abrupt Variations". In: *Proc. European Signal Process. Conf. (EUSIPCO)*. Kos, Greece, Sept. 2017, pp. 2442–2446.

National conferences

[TDT15b] P.-A. Thouvenin, N. Dobigeon, and J.-Y. Tourneret. "Estimation de variabilité pour le démélange non-supervisé d'images hyperspectrales". In: *Actes du XXVième Colloque GRETSI*. in French. Lyon, France, Sept. 2015.

List of publications III

[TDT17a] P.-A. Thouvenin, N. Dobigeon, and J.-Y. Tourneret. "Une approche distribuée asynchrone pour la factorisation en matrices non-négatives – application au démélange hyperspectral". In: *Actes du XXVIième Colloque GRETSI*. in French. Juan-les-Pins, France, Sept. 2017.

Back to main slide